International Journal of Greenhouse Gas Control 136 (2024) 104186

Contents lists available at ScienceDirect

International Journal of Greenhouse Gas Control

journal homepage: www.elsevier.com/locate/ijggc

Corrosion performance of A3 carbon steel in 30wt.% MEA and AMP-MEA blends for post-combustion carbon capture: Effect and mechanism of corrosion inhibitors

Yuwei Wang [a], Mengxiang Fang [a,b,*], Jun Gao [c], Chao Li [a], Yan Huang [c], Lin Yang [c], Shuifei Li [c], Ximing Hu [b], Tao Wang [a,b]

[a] State Key Laboratory of Clean Energy Utilization, Zhejiang University, Hangzhou 310027, China
[b] Qingshanhu Energy Research Center, Zhejiang University, Hangzhou 311300, China
[c] Guoneng Jinjie Energy Co., Ltd., Yulin 719000, China

ARTICLE INFO

Keywords:
Amine-based solvent
Corrosion
Carbon steel
Electrochemical test
Carbon capture

ABSTRACT

The corrosion behavior of A3 carbon steel in 30 wt.% MEA and AMP-MEA (2:1) blended amine solutions, two typical CO_2 capture solvents for chemical absorption processes, was investigated. The inhibition effects of imidazoline, sodium metavanadate ($NaVO_3$), and phosphoric acid, triethanolamine salt (P-TEA) were evaluated using various electrochemical testing techniques and immersion corrosion experiments. Results showed that $NaVO_3$ exhibited the highest corrosion inhibition effect at a concentration level of 1000 ppm, while imidazoline showed limited effectiveness. Both $NaVO_3$ and P-TEA significantly increased solution resistance and charge transfer resistance, thereby enhancing corrosion inhibition. Additionally, AMP-MEA blends exhibited improved corrosion performance compared to MEA, with the formation of a denser protective layer on the surface of A3 carbon steel. Furthermore, experimental results revealed that $NaVO_3$ and P-TEA, instead of forming protective oxide or carbonate layers, formed complexes or chelates with iron ions in the solution. These compounds adsorbed onto the carbon steel surface, effectively preventing further corrosion. These findings provide valuable insights into the corrosion behavior of A3 carbon steel in amine-CO_2–H_2O systems and underscore the potential of $NaVO_3$ and P-TEA as effective corrosion inhibitors. This knowledge is crucial for developing enhanced corrosion control strategies in related industrial applications.

1. Introduction

Carbon capture, utilization and storage (CCUS) is considered one of the most promising technologies for reducing CO_2 emissions. Among its various approaches, post-combustion CO_2 capture (PCCC) is particularly noteworthy for its potential applicability to existing plants and power stations. (A. Kohl and R. Nielsen, 2007; Intergovernmental Panel on Climate Change, 2011; Romeo et al., 2008). Single or blended organic amine aqueous solutions are widely used in chemical absorption carbon capture systems due to their cost-effectiveness and high flue gas treatment capacity(M.J. Al-Marri, 2017; Saeed et al., 2018; Tsouris and Aaron, 2005). However, the presence of carbonate, bicarbonate, and carbamate species in CO_2-loaded amine solutions significantly increases the corrosive tendency when in contact with carbon steel, which is a more economical alternative to stainless steel for construction materials. (Gao et al., 2012; Liu et al., 2019; Soosaiprakasam and Veawab, 2008; Zheng et al., 2016b). Additionally, the long-term circulation of amine solutions in the system, coupled with exposure to high temperatures and impurities in flue gasses (such as O_2, SOx, and NOx), induces degradation reactions. This results in the formation of heat stable salts (HSSs), which further accelerate the corrosion process. (Xiang et al., 2015, Y. 2014).

Many studies have investigated the corrosion mechanism occurring at the interface between the amine-CO_2–H_2O solution and the carbon steel surface (Sadeek et al., 2018; Veawab and Aroonwilas, 2002; Zhao et al., 2023a; Zheng et al., 2014). In this system, the anodic reaction during the corrosion process is iron dissolution, as shown in Eq. (1).

$$Fe \leftrightarrow Fe^{2+} + 2e^{-} \quad (1)$$

The cathode reactions in a CO_2-loaded amine solution are intricate

* Corresponding author.
E-mail address: mxfang@zju.edu.cn (M. Fang).

https://doi.org/10.1016/j.ijggc.2024.104186
Received 9 May 2023; Received in revised form 6 June 2024; Accepted 15 June 2024
Available online 25 June 2024

due to the presence of various species, including hydrogen ions (H^+), carbonic acid (H_2CO_3), carbonate (CO_3^{2-}), bicarbonate (HCO_3^-), and carbamate (RNH_2COO^-). This system, characterized by a relatively high pH, results in low concentrations of H^+ and H_2CO_3 (Kittel and Gonzalez, 2014; Kladkaew et al., 2009). The cathodic reactions, outlined in Eqs. (2-5), exemplify this complexity. The overall corrosion performance of amine-CO_2 solution depends on the quantity and types of oxidants and intermediates in the system, as well as the characteristics of corrosion products (Fytianos et al., 2016, G. 2014; Tang et al., 2017; Yu et al., 2017).

$$2HCO_3^- + 2e^- \leftrightarrow 2CO_3^{2-} + H_2 \quad (2)$$

$$2H_3O^+ + 2e^- \leftrightarrow H_2 + 2H_2O \quad (3)$$

$$2H_2O + 2e^- \leftrightarrow H_2 + 2OH^- \quad (4)$$

$$O_2 + 2H_2O + 4e^- \leftrightarrow 2CO_3^{2-} + H_2 \quad (5)$$

To address the corrosion issue, it is essential to prevent the electrochemical reactions occurring on the metal surface. Inhibiting either the anodic or cathodic reaction can effectively slow down galvanic corrosion. These inhibitors are categorized as cathodic, anodic, or mixed corrosion inhibitors based on their impact on the electrodes (Zhao et al., 2023a). Anodic corrosion inhibitors function through the following actions: 1) Formation of a dense oxide film with strong adhesion on the metal surface. As the oxide film reaches a certain thickness, the rate of oxidation reaction slows down. 2) Effective inhibition of the ionic process of metal through characteristic adsorption. 3) Adjustment of the metal electrode potential to reach the passivation potential(Ahn et al., 2010; Emori et al., 2017). Cathodic corrosion inhibitors increase the polarization of the cathodic process by eliminating or reducing the depolarizing agent, thereby slowing the corrosion(Schweitzer, 2017). Mixed corrosion inhibitors can simultaneously decrease the reaction rate of both the anode and cathode, mainly through adsorption on both electrodes, forming an insoluble protective film that isolates the metal from the corrosive medium (Hermas et al., 2019; Yadav et al., 2014).

Lu et al. investigated the corrosiveness of a specific amine solution on carbon steel coupons and conducted corrosion experiments using three imidazoline quaternary ammonium salt corrosion inhibitors (LU et al., 2021). The results indicated that, for CO_2-saturated solutions at 100 °C −120 °C, the corrosion inhibition efficiency exceeded 99% when the inhibitor was present at a concentration of 1000 mg/L. Furthermore, Previous studies have demonstrated the significant corrosion inhibition efficiency of vanadium compounds (VND). In the presence of oxygen, $NaVO_3$ exhibits an outstanding corrosion inhibition efficiency of up to 98% for the MEA-piperazine system (Ma et al., 2022). Chen et al. investigated the influence of three phosphate corrosion inhibitors (Na_2PO_3F, Na_2HPO_4, Na_3PO_4) on chloride ion binding and established a modified chloride binding isotherm. The results demonstrated that during the ion exchange process, phosphates exhibited higher priority over chlorides. The addition of phosphate corrosion inhibitors effectively reduced chloride concentrations (Chen et al., 2020). Nahali et al. investigated the influence of phosphate inhibitor on the corrosion performance of steel immersed in 3% NaCl solution. Their findings revealed a high phosphate content in the fortified area, where the passive layer formed on the metal surface effectively protected the steel against localized corrosion (Nahali et al., 2015).

The selection of the three inhibitors in this study was based on their well-documented effectiveness as corrosion inhibitors. However, their performance in organic amine solutions has not been extensively studied. Therefore, this study aimed to fill this gap and provided insights into the corrosion behavior of A3 carbon steel in CO_2 capture solvents. The names and structural formulas of three corrosion inhibitors used in this study are shown in Table 1. The simple corrosion inhibition principles of the three inhibitors are introduced below.

$NaVO_3$: anodic corrosion inhibitor. It inhibits the anodic reaction by forming a dense oxide or hydroxide oxide film on the metal surface. This protective film effectively prevents the metal from dissolving into the water and facilitates the passivation of the anode(Zhao et al., 2023b). $NaVO_3$ is a commonly used corrosion inhibitor in the amine-based CO_2 capture process, typically applied at concentrations ranging from 1000 to 10,000 ppm(Gao et al., 2012).

Table 1
Name and structural formula of corrosion inhibitors.

Name	CAS number	Structural formula
Sodium metavanadate ($NaVO_3$)	13718-26-8	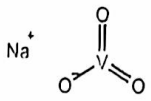
Imidazoline	504-74-5	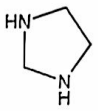
Phosphoric acid, triethanolamine salt (P-TEA)	10017-56-8	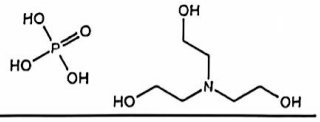

Imidazoline: mixed corrosion inhibitor. Imidazoline can be adsorbed on the metal surface to form a relatively stable liquid film, which can change the REDOX potential of hydrogen ions, and can also complex some oxidants in the solution. Imidazoline-based corrosion inhibitors are widely used in environments prone to CO_2/H_2S corrosion, and are commonly employed for corrosion protection in CO_2 flooding systems of the oil industry (Zhang et al., 2015).

Phosphoric acid, triethanolamine salt (P-TEA): mixed corrosion inhibitor. It prevents the corrosive medium from contacting the steel surface. Phosphate and triethanolamine groups can combine with iron ions to form insoluble chelate complex, which acts as a protective barrier on the metal surface. Phosphate-based corrosion inhibitors are frequently used for corrosion protection in water supply pipelines and marine environments (Ma et al., 2022).

Furthermore, different amine structure exhibits distinct corrosive behavior due to the CO_2 absorption mechanism and the formation of bicarbonates. Primary and secondary amines usually show significant corrosive tendencies while tertiary and sterically hindered amine do not [2]. Monoethanolamine (MEA), a primary amine, is widely used in PCCC plants for its efficient reaction kinetics and 30 wt.% MEA aqueous solution is a baseline for solvent performance. 2-amino-2-methyl-1-propanol (AMP), a sterically hindered form of MEA, was reported to display a better CO_2 loading capacity and higher thermal stability. Many studies have found that AMP-MEA blends showed both the fast reaction kinetics characteristic of primary amine, and the high loading capacity of sterically hindered amine. But the corrosive behavior of amine blends only has been reported by limited research. Shoukat studied the corrosion of stainless steel in tertiary amine blends and founded that Amine-MEG (monoethylene glycol) blends had lower metal concentrations than Amine-H_2O and Amine-TEG (triethylene glycol) blends, which indicated the lower corrosion rate (Shoukat and Knuutila, 2020). Zheng found that the average corrosion rate of AMP system was lower than that of the MEA system due to the difference of the corrosion products (Zheng et al., 2016b). Veawab reported that the corrosion products of the AMP system formed on the metal surface were harder than those of the MEA system (Veawab et al., 1997). Gunasekaran found that under CO_2 saturation at 80 °C, the corrosivity order was MEA>AMP≈MEA-AMP, and corrosion rate of MEA system was about 4 mm per year (mmpy) while that of AMP and MEA-AMP blends was approximately 3mmpy (Gunasekaran et al., 2013). Yu studied the corrosion behaviors of various kinds of single component amine solutions and amine blends at 120 °C. Increased concentration of tertiary or sterically hindered amine

to primary or secondary amine precipitated more $FeCO_3$, leading to reduced corrosion Amines with either tertiary or sterically hindered molecular structures were the basis for promotion of carbonate ions in solution leading to the formation of siderite. (Yu et al., 2016).

In the present study, the corrosivity of aqueous amine solutions comprising both 30 wt.% MEA and AMP-MEA blends was studied. The corrosion inhibition performance of the three typical corrosion inhibitors at a concentration of 1000 ppm was evaluated through immersion corrosion experiments at 100 °C. HSSs anion and iron ion concentration in the solution were measured to monitor the composition change of the solvent. Surface analytical techniques (scanning electron microscopy [SEM], X-ray diffraction [XRD]) were also applied to obtain the surface morphology and chemical composition of corrosion products. Furthermore, corrosion behavior was experimentally evaluated using electrochemical techniques (polarization curves, and electrochemical impedance spectroscopy [EIS] measurement).

2. Experimental apparatus and methods

2.1. Materials

This paper is focused on immersion corrosion and electrochemical research on A3 carbon steel (ASTM A3). The chemical composition of the steel is presented in Table 2. According to ASTM standards, the size of carbon steel sample was 10mm*2mm*20 mm. Prior to the experiment, all carbon steel samples were abraded with 240 mesh and 500 mesh SiC sandpaper grinding to the surface bright without protective film (ASTM, 1999). Ultrasonic cleaning was then performed with deionized water and methanol. Ethanolamine (MEA) and 2-Amino-2-methyl-1-propanol (AMP) stock solution was provided by Macklin (>99.5%). MEA and AMP-MEA (mass ratio: 2:1) blended aqueous solutions were prepared by weight with a total amine concentration of 30 wt.% and the balance was ultra-pure water. The prepared solutions were placed in three-necked flat-bottom flasks under a water bath at 40 °C fitted with reflux condenser. CO_2–N_2 mixture gas (CO_2vol fraction = 12%) was steadily bubbled through the solution for hours. The outlet gas of the reflux condenser was directed into an infrared CO_2 gas analyzer for real-time monitoring of CO_2 concentration. The constant CO_2 concentration in the outlet gas indicated that the solution had reached CO_2 saturation. The corrosion inhibitors shown in Table 1 were separately added to the amine CO_2-saturated solutions at the beginning of the immersion experiments. $NaVO_3$ was provided by Macklin (>99.9%), imidazoline and phosphoric acid, triethanolamine salt were provided by Shandong Usolf with concentrations of 8% and 80%, respectively. The corrosion inhibitors were added at the concentration of 1000 ppm.

2.2. Immersion corrosion experiment

After weighed, the polished carbon steel sample was put into the Teflon (PTFE) liner of the high-temperature and high-pressure reactor kettle shown in Fig. 1, and completely submerged into 20 mL CO_2-saturated solution to ensure that the liner was filled with no air trapped. Then, the reactor was numbered according to the sampling time and tightened with grip bar to ensure the tightness. The reactor was placed in the oven and heated to the experimental temperature of 100 °C. The corresponding reactor was taken out of the oven at specific intervals (2d, 4d, 7d, 14d, 21d, 28d), and the solution sample was collected for subsequent HSS and iron ion concentration analysis.

According to the ASTM standard, 500 mL detergent containing 265 mL hydrochloric acid (HCl, sp gr 1.19) and 1.75 g methenamine (the balance was ultra-pure water) was prepped. The carbon steel sample was immersed in the detergent for 30 min to remove the corrosion products (including protective film) on the surface(ASTM Standard, 2011). Thereafter, the sample was washed by deionized water and methanol, then dried and weighed. Corrosion rate R is calculated by Eq. (6):

$$R = 8760 \cdot 10^3 (m_0 - m_1) \; / \; St\rho \tag{6}$$

Where m_0 and m_1 are the weight of the sample piece before and after corrosion, g; S is surface area of carbon steel sample, mm^2; t is the corrosion test duration, h; ρ is the density of carbon steel, $g{\cdot}cm^3$.

Moreover, to minimize experimental error, three reactors under identical conditions were employed for each batch of experiments, with each reactor accommodating a single carbon steel sample. In addition to weight loss measurement, one sample from each batch was designated for XRD and SEM analysis.

2.3. Characterization methods

To characterize the corrosion products of A3 carbon steel in the amine-CO_2–H_2O solution, XRD analysis was conducted. All XRD scans were performed using Nikko Smartlab 9kw equipped with a Cu target with a wavelength of 0.15406 nm, operating voltage EIS of 40 kV, current of 40 Ma, scanning step size of 0.0262606, using θ/2-θ mode with the detector's 2-θ range of 10 to 80° For the XRD analysis, the carbon steel sample was prepared as follows: The corroded surface was carefully cleaned to remove any loose debris or contaminants. Then the sample was mounted on suitable substrates using an epoxy resin to ensure stability during analysis.

Hitachi Regulus8100 scanning electron microscope was used to characterize the surface morphology of the carbon steel sample. The scanning voltage was 10–20 kV and the current was 0.4nA. Regarding SEM analysis, the preparation method involved the following steps: After cleaning the carbon steel sample to remove any surface contaminants, it was carefully mounted onto SEM stubs using a conductive adhesive to ensure proper electrical conductivity. The prepared sample was transferred to the SEM chamber for analysis.

To better analyze the degradation of the solution during the corrosion process, Ion Chromatography (IC) test analysis of the solution sample was necessary. All anion analysis tests were performed using Metrohm 940 Professional IC, using Metrosep A Supp 7–250/4.0 separation column. The solution sample was diluted prior to injection at dilution ratios ranging from 50 to 100. The eluent was eluted with 3.6 mmol/L sodium carbonate solution at a flow rate of 0.7 ml/min by isocratic elution. The test time of a single sample was 40 min. Because of the CO_2 inhibition module of the instrument, carbamate, and carbonate ions in the organic amine solution with high CO_2 loading did not affect the peak time and peak shape of the tested anions.

In addition, to understand the level of iron ions in the solution, Inductively Coupled Plasma Optical Emissions Spectroscopy (ICP-OES) tests were performed on the solution using Agilent 7700. To gain further insights into the impact of HCO_3^- concentration on the corrosion process in both absorbent systems, characterization of the solution sample was conducted using 13C NMR (JNM-ECZ600R/S1). In this analysis, D_2O was employed as an internal standard for deuterium lock (Zhou et al., 2016).

2.4. Electrochemical test

A typical three-electrode system was used for electrochemical test,

Table 2
Composition of A3 carbon steel sample, wt.%.

Element	C	Si	Mn	Cr	Mo	Ni	Cu	V	P	S	Fe
Content	0.20	0.29	0.83	0.19	0.11	0.18	0.23	0.005	0.041	0.045	Bal

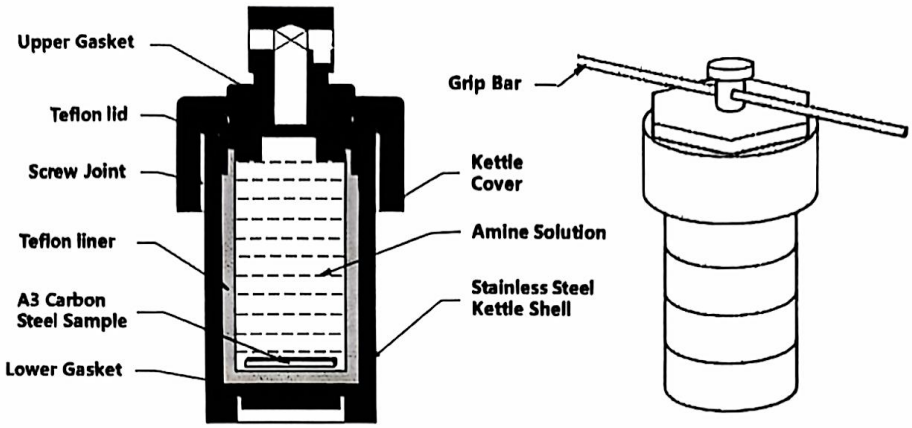

Fig. 1. High-temperature and high-pressure reactor for immersion corrosion test.

comprising a platinum (Pt) electrode as the counter electrode (CE), a single salt bridge mercury oxide electrode as the reference electrode (RE), and a carbon steel sample measuring 10 × 20 × 2 mm as the working electrode (WE). Prior to the experiment, the working electrode was polished with sandpaper (250 mesh, 500 mesh, 800 mesh), then washed with deionized water and methanol to keep clean, and finally dried. The three electrodes were placed in the amine solution. The CO_2 loading of 30 wt.% MEA and AMP-MEA blended solution was 0.46 mol/mol (C/N) and 0.65 mol/mol (C/N), respectively.

The electrochemical performance of the working electrode was evaluated using a Chenhua CHI600E series electrochemical workstation. Before the experiment, an open-circuit voltage test was conducted to determine the self-etching potential (E_{corr}) of the working electrode, which was recorded once the voltage had stabilized.

The potentiodynamic polarization technique was then employed with a scanning speed of 1 mV/s. The initial and final voltages were set at −0.5 and +1.25 V vs E_{corr}, respectively. Subsequently, the Tafel curve, delineating the correlation between current density and electrode potential, was derived through a sequential scan. To determine the corrosion potential and current, the Tafel extrapolation method was employed. This involved extending the linear portions of the cathodic and anodic polarization curves until they intersected at a single point, as described in the literature. (Sedik et al., 2022; Stansbury and Buchanan, 2000).

Furthermore, A.C impedance technique was applied with an initial voltage set at E_{corr}, and a frequency range of 0.1 Hz to 100 kHz. This technique measured the impedance response of the electrochemical system under an alternating potential or current, providing EIS data.

3. Results and discussion

3.1. Immersion experiment

3.1.1. Inhibition effect in 30wt.% MEA solution

The immersion corrosion test at 100 °C evaluated the corrosion rate of A3 carbon steel in the MEA solution with 1000 ppm various corrosion inhibitors over an extended period. This approach allowed for a preliminary assessment of the effectiveness of various corrosion inhibitors. Fig. 2 illustrates the corrosion rate variation of A3 carbon steel over a four-week period under the influence of different corrosion inhibitors, as determined by the weight loss method outlined in Eq. (6). All solutions exhibited a rapid decline in corrosion rates within the first week and tended to stabilize after approximately two weeks. This behavior indicated that a protective film layer formed on the carbon steel surface, reaching near-complete coverage after two weeks of immersion, resulting in a relatively stable and low corrosion rate thereafter.

Notably, the MEA solution without corrosion inhibitor exhibited the most pronounced corrosion rate, reaching nearly 0.5 mmpy after 2 days and significantly reducing to approximately 0.05 mmpy after four weeks. In contrast, $NaVO_3$ and P-TEA demonstrated superior corrosion inhibition effects in the MEA solution. Specifically, the corrosion rate with $NaVO_3$ was only 0.067 mmpy after two days, further decreasing to about 0.003 mmpy after two weeks. Conversely, imidazoline proved less effective in inhibiting corrosion, with corrosion rates of 0.0643 mmpy and 0.0868 mmpy in the MEA aqueous solution with and without imidazoline, respectively, representing a poor inhibition efficiency of approximately 26%.

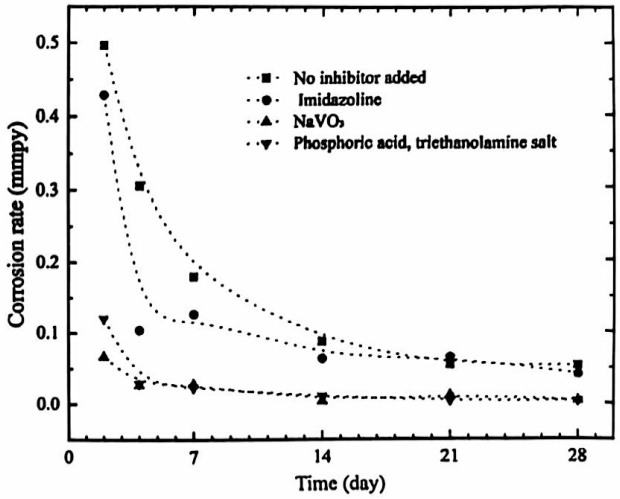

Fig. 2. Corrosion rates of A3 carbon steel in 30 wt.% MEA with different corrosion inhibitor added at 100 °C, obtained by immersion corrosion experiments (CO_2-loading 0.46 mol/mol).

To summarize, in the MEA solution system, the corrosion inhibition effectiveness of the three corrosion inhibitors at a concentration of 1000 ppm ranks as follows: $NaVO_3$ > P-TEA > imidazoline. However, it is important to note that the amine solution in this experiment was static, deviating from the actual operational conditions of industrial carbon capture devices. In practical applications, flowing solutions can cause some degree of damage to the protective film formed, resulting in reported corrosion rates in chemical absorption systems being typically at least an order of magnitude higher. (Cousins et al., 2013; Liu and Rochelle, 2022; Zhao et al., 2011; Zheng et al., 2016a).

3.1.2. Inhibition effect in 30wt.% AMP-MEA blended solution

As shown in Fig. 3, the corrosion resistance of the AMP-MEA blended

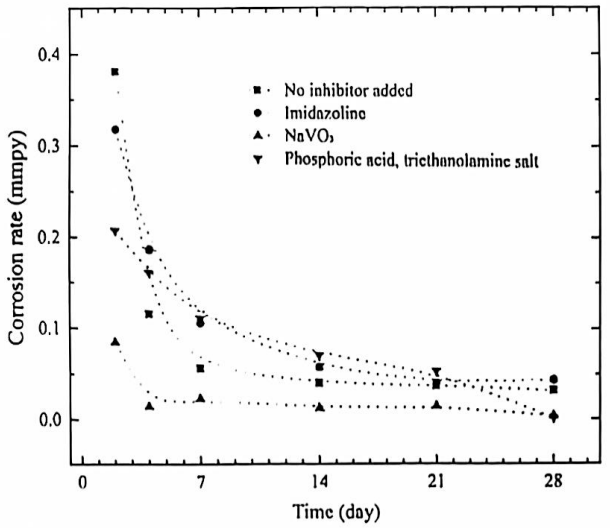

Fig. 3. Corrosion rates of A3 carbon steel in 30 wt.% AMP-MEA with different corrosion inhibitor added at 100 °C, obtained by immersion corrosion experiments (CO_2-loading 0.61 mol/mol).

solution exhibited an improvement when compared to that of the MEA solution. The corrosion rates of carbon steel in the AMP-MEA solution were observed to be lower compared to those in the MEA solution. However, the trend was similar, with corrosion rates stabilizing after approximately two weeks. The reduced corrosion rate in the AMP-MEA system could be attributed to the sterically hindered nature of AMP. As shown in Eq. (7-8), $AMPCOO^-$, the main product after CO_2 absorption, exhibited poor stability and was easily hydrolyzed to AMP and HCO_3^-, so the HCO_3^-/CO_3^{2-} concentration was an order of magnitude higher than that of the MEA solution (Zheng et al., 2016b). Therefore, $FeCO_3$ (siderite), $Fe_2(OH)_2CO_3$ (chukanovite) and other protective layers would be rapidly formed on the surface of carbon steel in this solution, thereby inhibiting corrosion (Campbell et al., 2016; Koo and Kim, 2020; Lee and Wilkin, 2010; Pandarinathan et al., 2014).

$$CO_2 + 2AMP \leftrightarrow AMPCOO^- + AMPH^+ \quad (7)$$

$$AMPCOO^- + H_2O \leftrightarrow AMP + HCO_3^- \quad (8)$$

Regarding the impact of the three corrosion inhibitors, imidazoline exhibited even negative effect, with the corrosion rate slightly exceeding that of the solution without a corrosion inhibitor. $NaVO_3$ demonstrated the most robust inhibition effect, yielding a corrosion rate of only 0.0035 mmpy after four weeks, corresponding to an inhibition efficiency of at least 89%. P-TEA exhibited a noticeable corrosion inhibition effect on carbon steel from the second day, reducing it by approximately half compared to the system without a corrosion inhibitor. Compared to $NaVO_3$, the variation in corrosion rate with P-TEA appeared to follow a more linear trend. This suggested that the corrosion inhibition effectiveness of P-TEA in AMP-MEA blended solution had a prolonged onset period, indicating a slower rate of complexation between P-TEA molecules and iron ions in the solution. The speed at which different corrosion inhibitors exerted their effects was closely tied to their chemical structures and corrosion inhibition mechanisms. This underscored the importance of further research in this area for the future design and optimization of corrosion inhibitors.

3.2. Solution degradation and HSSs analysis

Previous studies have shown that HSS accumulated in the solution has a certain influence on the corrosion process, and different HSS ions have different effects on the corrosion. The presence of HSS in the solution may increase the solubility of iron ions in the amine solution and increase the conductivity of amine aqueous solution, leading to the intensification of corrosion (Rooney and Dupart, 2000; Soosaiprakasam and Veawab, 2008; Veawab and Aroonwilas, 2002).

Figs. 4 and 5 show the concentration levels of HSS ions in MEA and AMP-MEA solutions following the four-week immersion corrosion experiment. Except for acetate, the concentrations of glycolic, formic, sulfuric, and oxalate anions all exceeded 100 ppm.

In the MEA solution, the three corrosion inhibitors partially inhibited the solvent degradation process, with P-TEA exhibiting the most pronounced effect. In the AMP-MEA solution, the HSS content increased in the imidazoline and P-TEA systems. $NaVO_3$ demonstrated the most favorable impact on the degradation of both solutions when employed as a corrosion inhibitor.

Furthermore, the ICP results showed that the concentration of iron ions in the solution without a corrosion inhibitor fluctuated between 40 and 50 ppm over 4 weeks. In the $NaVO_3$ and P-TEA systems, that the concentration of iron ions was between 30 and 40 ppm. This indicated that the three corrosion inhibitors had no significant effect on controlling the overall concentration of iron ions in the amine solution. In fact, the inhibitors did not directly block the dissolution process of iron ions in the liquid phase. Instead, the inhibitors preemptively chelated with iron ions dissolved in the solution, forming iron complex that adsorbed to the surface of the carbon steel and blocked the reaction (Sadeek et al., 2018). The presence of free iron ions could partly catalyze the degradation reaction of the solution, so the corrosion inhibitors also inhibited the degradation and reduce the concentration of HSS ions in the solution to a certain extent.

3.3. Corrosion products and SEM analysis

Figs. 6 and 7 show the XRD results of A3 carbon steel in the immersion corrosion experiments. It could be found that $Fe_2(OH)_2CO_3$ protective layer was formed on the surface of carbon steel sample in the MEA and AMP-MEA amine solutions without corrosion inhibitor and with imidazoline added. $NaVO_3$ and P-TEA systems showed no discernible corrosion products. This indicated that the amine solution with imidazoline had undergone intense corrosion processes like the solution without inhibitor, leading to the formation of corrosion products. In fact, the corrosion inhibition effect of imidazoline arises from the active sites on its five-membered ring, and these molecules can form coordinate and back-donating bonds with atoms on metal surface. (Yan et al., 2013; Zhang et al., 2010) However, in high-temperature alkaline environments, imidazoline is highly susceptible to hydrolysis, resulting

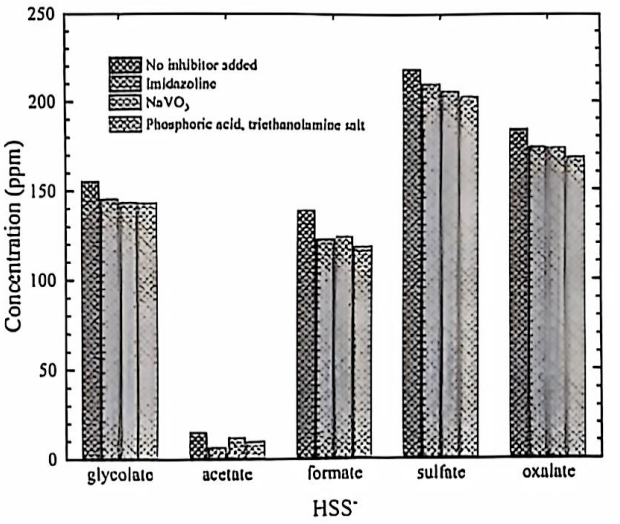

Fig. 4. HSS level of 30 wt.% MEA solution after four-week immersion corrosion at 100 °C.

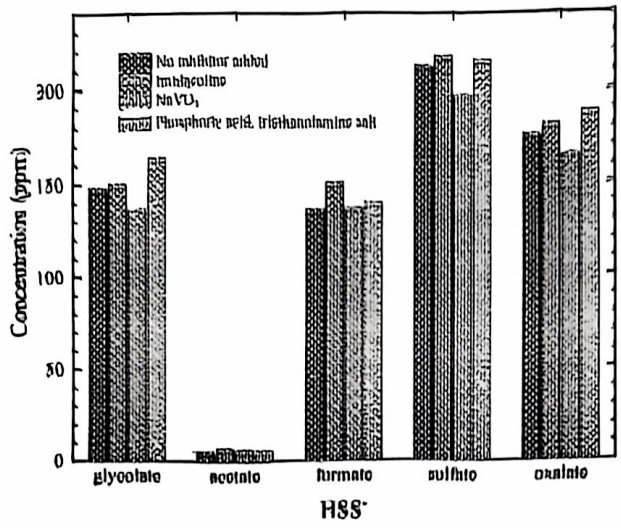

Fig. 5. HSS level of 30 wt.% AMP-MEA solution after four-week immersion corrosion at 100 °C.

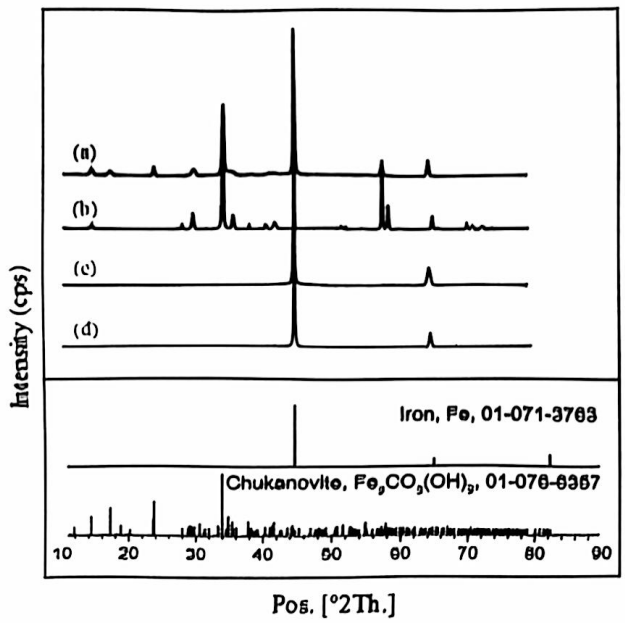

Fig. 6. XRD of corrosion products on the surface of A3 carbon steel after immersion corrosion in MEA solution for four weeks (a: No inhibitor; b: Imidazoline; c: $NaVO_3$; d: P-TEA).

in ring-opening and the formation of amides, consequently leading to a significant decline in its corrosion inhibition efficiency (Tie et al., 2017; Zhu et al., 2002). Therefore, we inferred that imidazoline was better suited for application in acidic environments such as CO_2 aqueous solutions, rather than in alkaline organic amine solvents.

The SEM images in Fig. 8 also clearly reveal the microstructure of $Fe_2(OH)_2CO_3$ layer, and the layer formed in the AMP-MEA solution was denser, which also verified the conclusion in Section 3.1.2. According to previous studies, $Fe_2(OH)_2CO_3$, rather than $FeCO_3$, formed on the surface of carbon steel when the CO_2 loading in solution was very high and it was in an anoxic corrosion environment (Saheb et al., 2014; Schlegel et al., 2010). The environmental conditions of carbon steel reported in the literature for the formation of $Fe_2(OH)_2CO_3$ were consistent with the experimental conditions in this study (Lee and Wilkin, 2010;

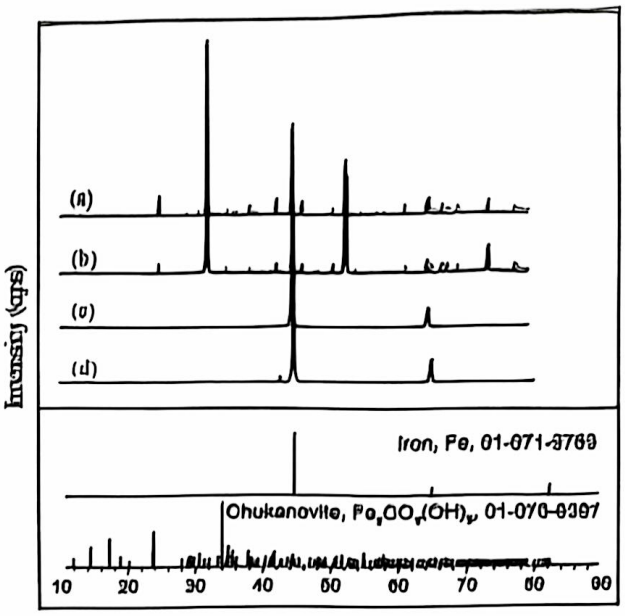

Fig. 7. XRD of corrosion products on the surface of A3 carbon steel after immersion corrosion in AMP-MEA blended solution for four weeks (a: No inhibitor; b: Imidazoline; c: $NaVO_3$; d: P-TEA).

Pandarinathan et al., 2014; Zhang et al., 2016a).

3.4. Electrochemical corrosion behavior

3.4.1. Corrosion potential and current

In a corrosive environment, there exists a discernible correlation between corrosion potential and corrosion propensity, while corrosion current density is intimately linked to corrosion rate (Zhou et al., 2017). Fig. 9 illustrates the Tafel curves of the carbon steel sample immersed in a CO_2-saturated MEA solution with the three corrosion inhibitors. Table 3 shows the electrochemical parameters fitted by Tafel curves, where E_{corr} is corrosion potential (V), I_{corr} is corrosion current (A), and J_{corr} is corrosion current density (mA/cm^2). Compared to the MEA solution without corrosion inhibitor added, the corrosion potential of carbon steel increased to varying degrees with the addition of any corrosion inhibitor. The corrosion potential of carbon steel without an inhibitor was −0.661 V. In contrast, with the addition of imidazoline and P-TEA, the corrosion potential rose to approximately −0.220 V, and with $NaVO_3$, it increased most significantly to −0.042 V.

Fig. 10 and Table 4 respectively show the Tafel curve and fitting parameters of carbon steel samples in CO_2-saturated AMP-MEA solution. The corrosion potential observed in the AMP-MEA blended solution was consistently higher compared to that in the MEA solution. This signified that the corrosion process of carbon steel in the AMP-MEA solution was less prone to occur, demonstrating stronger corrosion resistance compared to the MEA solution. Moreover, all three corrosion inhibitors demonstrated an ability to enhance the corrosion potential in both amine solutions, underscoring their positive corrosion inhibition effects.

Nonetheless, the three inhibitors exhibited limited effect in reducing corrosion current density. In the MEA solution, only the addition of P-TEA led to a significant decrease in corrosion current density, registering an 86% reduction compared to the system without a corrosion inhibitor. Conversely, the corrosion current density in solutions with $NaVO_3$ and imidazoline saw slight increases. In AMP-MEA solution, the corrosion current density experienced slight increases with imidazoline and P-TEA, while it marginally decreased with $NaVO_3$. It is crucial to note that these experiments were conducted after subjecting the carbon steel sample to 60 h of pre-corrosion in the amine solution at 40 °C. The

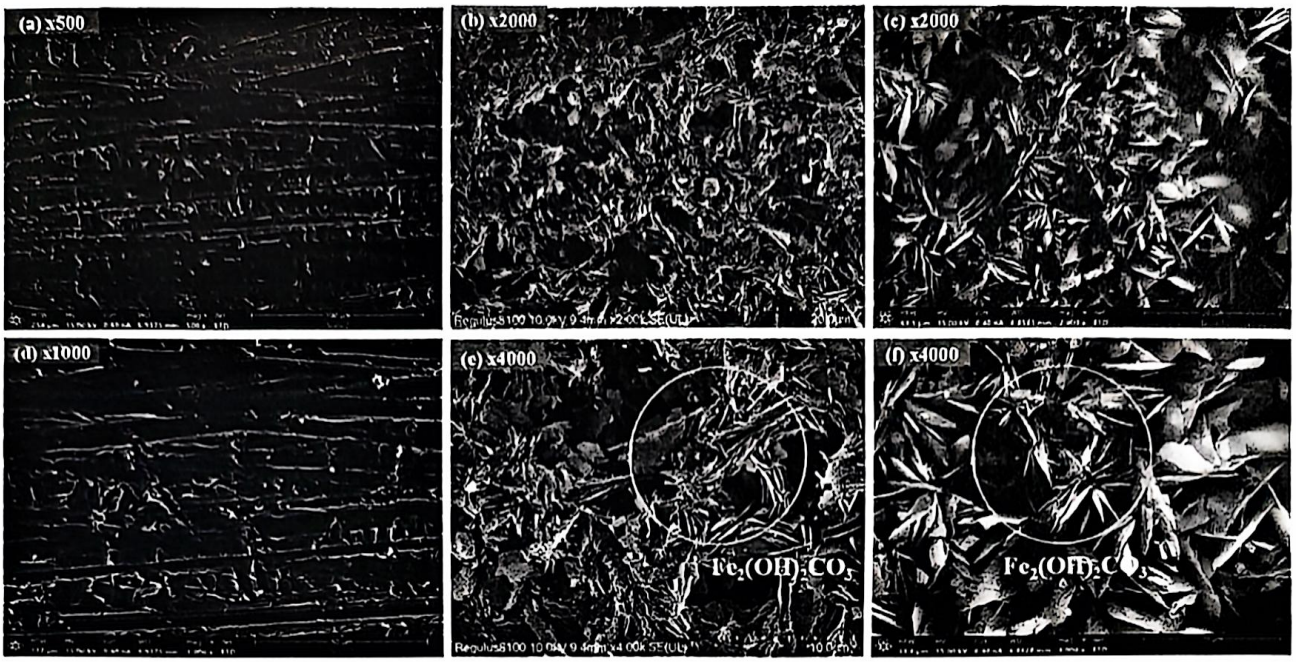

Fig. 8. SEM image of corroded carbon steel sample surface (a, d: Initial carbon steel; b, e: MEA; b, d: AMP-MEA).

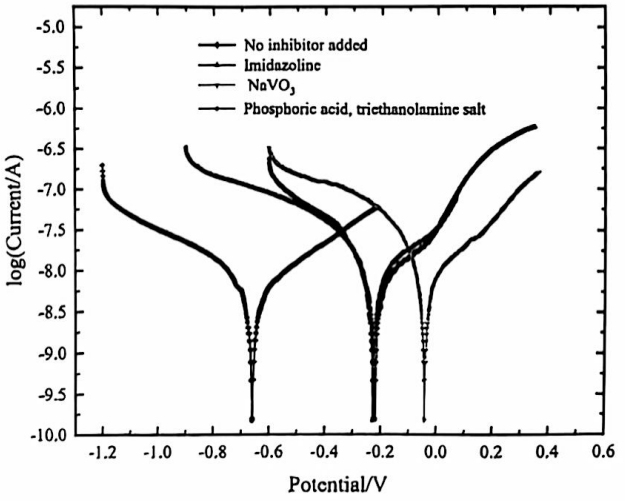

Fig. 9. Tafel curve of A3 carbon steel sample in 30 wt.% MEA solution with different corrosion inhibitor added (pre-corroded for 60 h, CO_2-loading 0.46 mol/mol).

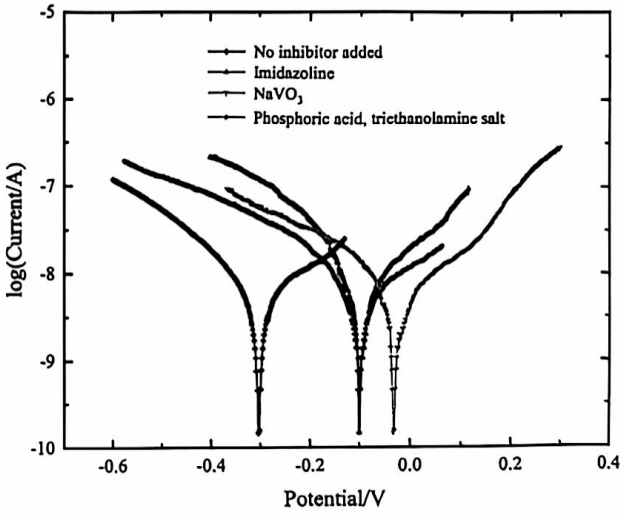

Fig. 10. Tafel curve of A3 carbon steel sample in 30 wt.% AMP-MEA blended solution with different corrosion inhibitor added (pre-corroded for 60 h, CO_2-loading 0.61 mol/mol).

Table 3
Fitting parameters of Tafel curve of carbon steel sample in 30 wt.% MEA solution.

Inhibitor	E_{corr} / V	I_{corr} / A	J_{corr} / mA·cm^{-2}
No inhibitor	−0.661	8.061E-09	1.55E-06
Imidazoline	−0.220	9.402E-09	1.81E-06
$NaVO_3$	−0.042	1.037E-08	1.99E-06
Phosphoric acid, triethanolamine salt	−0.228	1.127E-09	2.17E-07

Table 4
Fitting parameters of Tafel curve of carbon steel sample in 30 wt.% AMP-MEA blended solution.

Inhibitor	E_{corr} / V	I_{corr} / A	J_{corr} / mA·cm^{-2}
No inhibitor	−0.304	8.205E-09	1.58E-06
Imidazoline	−0.099	8.859E-09	1.70E-06
$NaVO_3$	−0.033	8.032E-09	1.54E-06
Phosphoric acid, triethanolamine salt	−0.102	9.984E-09	1.92E-06

protective layer on the surface was not fully formed, rendering the corrosion potential and current density values suitable only for comparative analysis, not for calculating corrosion rates. In summary, $NaVO_3$ demonstrated the most optimal corrosion inhibition effect in both absorbent solutions, aligning with the subsequent immersion corrosion test results.

Nonetheless, the three inhibitors exhibited limited effectiveness in reducing corrosion current density. In the MEA solution, only the addition of P-TEA led to a significant decrease in corrosion current

density, registering an 86% reduction compared to the system without a corrosion inhibitor. Conversely, the corrosion current density in solutions with $NaVO_3$ and imidazoline slightly increased. In the AMP-MEA solution, the corrosion current density experienced slight increases with imidazoline and P-TEA, while it marginally decreased with $NaVO_3$. It is crucial to note that these experiments were conducted after immersing the carbon steel sample in the amine solution at 40 °C for 60 h. The protective layer on the surface was not fully formed, rendering the corrosion potential and current density values suitable only for comparative analysis, not for calculating corrosion rates. In summary, $NaVO_3$ demonstrated the most optimal corrosion inhibition effect in both absorbent solutions, aligning with the immersion corrosion test results.

3.4.2. EIS test

To further understand the electrochemical behavior of A3 carbon steel in the amine solutions, electrochemical impedance spectroscopy (EIS) was measured. The basic approach was to model the electrochemical system as an equivalent circuit composed of basic components such as resistance, capacitance, and inductance, arranged in series or parallel. The EIS curve could reflect the parameters of these components, facilitating a detailed analysis of the reaction process. Fig. 11 shows the equivalent circuit model of carbon steel in aqueous amine solution, which consisted of a charge-transfer resistance (R_p) and a constant-phase element (CPE) in parallel and both in series with a solution resistance (R_s). The R_s parameter represents the resistance of the electrolyte solution, while R_p reflects the resistance to charge transfer at the electrode-electrolyte interface.

The equivalent circuit expression of CPE, a constant phase angle element, is shown in the Eq. (9). The impedance of CPE is defined by two parameters, namely, CPE-T and CPE-P, where ω represents the angular frequency. The CPE component is introduced into the equivalent circuit model to account for non-ideal capacitive behavior often observed at electrode interfaces.

$$Z = \frac{1}{T \times (j\omega)^P} \tag{9}$$

Figs. 12 and 13 show the EIS of A3 carbon steel respectively not pre-corroded and pre-corroded for 60 h in the CO_2-saturated MEA solution. Table 5 and Table 6 show the fitting electrochemical parameters obtained through Zview software. The fitting process involved adjusting the parameters of the equivalent circuit model to minimize the difference between the measured and simulated impedance data, usually through iterative optimization algorithms. The impedance curves for both $NaVO_3$ and P-TEA systems displayed significant capacitive reactance, indicative of a low corrosion rate, which is consistent with the Tafel curve tests. In terms of charge transfer resistance, imidazoline exhibited the least significant increase. Coupled with its poorest corrosion inhibition performance observed in the immersion corrosion experiments, this indicated that the mitigating effect of imidazoline on corrosion in the alkaline environment was limited, unable to form a stable liquid film. Analyzing the parameter values of the equivalent circuit provided a more intuitive understanding of R_s in descending order: $NaVO_3$ > *P*-TEA > imidazoline > no inhibitor added. This demonstrated that the addition of these three corrosion inhibitors effectively increased solution resistance, although to varying degrees.

After a 60-hour pre-corrosion period, both R_s and R_p values increased across all systems. This rise could be attributed to the formation of a protective layer of corrosion products on the surface of the carbon steel sample. The presence of this layer impeded the charge transfer process of the carbon steel, increasing the difficulty for electrons to be transferred from the metal surface. This phenomenon indicated that, over time, the carbon steel developed increased resistance to corrosion. These findings were also in line with the results observed in the immersion corrosion experiments.

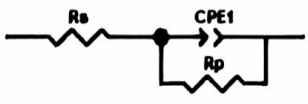

Fig. 11. EIS equivalent circuit for corrosion of A3 carbon steel in amine solution.

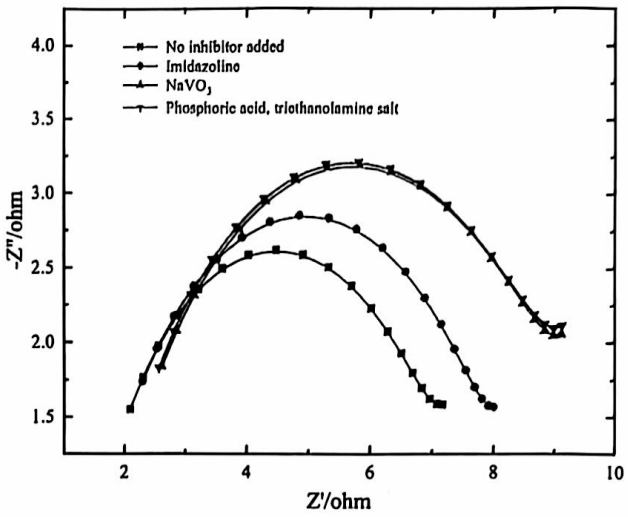

Fig. 12. EIS of A3 carbon steel in 30 wt.% MEA solution with different corrosion inhibitor added (no pre-corroded, CO_2-loading 0.46 mol/mol).

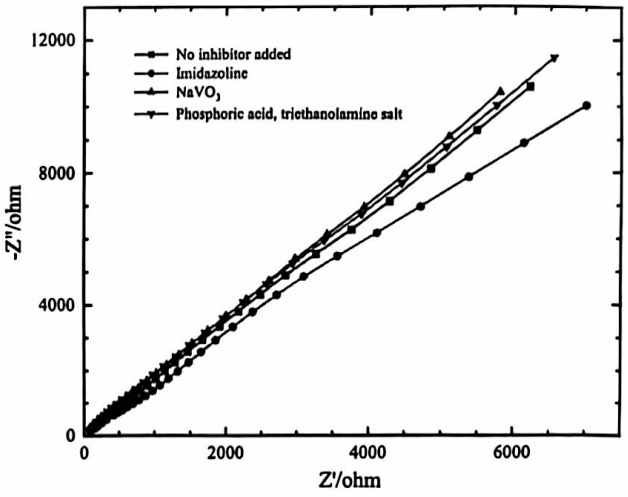

Fig. 13. EIS of A3 carbon steel in 30 wt.% MEA solution with different corrosion inhibitor added (pre-corroded for 60 h, CO_2-loading 0.46 mol/mol).

Table 5
Fitting electrochemical parameters based on EIS (no pre-corroded).

Inhibitor	R_s ($\Omega \cdot cm^2$)	R_p ($\Omega \cdot cm^2$)	CPE1-T ($10^{-6}\Omega^{-1}$ $S^n cm^{-2}$)	CPE1-P
No inhibitor	1.126	6.782	7.5558E-6	0.82683
Imidazoline	1.232	7.445	6.8664E-6	0.82719
$NaVO_3$	1.420	8.720	9.4202E-6	0.79727
Phosphoric acid, triethanolamine salt	1.391	8.747	9.0512E-6	0.80077

Table 6
Fitting electrochemical parameters based on EIS (pre-corroded for 60 h).

Inhibitor	R_s ($\Omega \cdot cm^2$)	R_p ($\Omega \cdot cm^2$)	CPE1-T ($10^{-6}\Omega^{-1}$ $S^n cm^{-2}$)	CPE1-P
No inhibitor	17.98	7047	1.6857E-7	0.77167
Imidazoline	25.14	10940	4.2903E-7	0.67952
$NaVO_3$	25.98	8021	1.1404E-7	0.80572
Phosphoric acid, triethanolamine salt	27.13	8487	1.1301E-7	0.81107

3.5. Corrosion and inhibition mechanism

According to the XRD and SEM analyses, valuable insights were gained regarding the reaction between the carbon steel and the solution during the corrosion process. Upon absorption of CO_2 by the organic amine solution, various species were formed, including carbamate, protonated amine, carbonic acid, bicarbonate, hydroxide, and hydrogen ions. Consequently, when the carbon steel sheet was immersed in the amine solution, the corrosion process involved both iron oxidation and the reduction reactions of bicarbonate, hydrogen ions, and water, as depicted in Eqs. (10-13).

$$Fe \leftrightarrow Fe^{2+} + 2e^- \quad (10)$$

$$2HCO_3^- + 2e^- \leftrightarrow 2CO_3^{2-} + H_2 \quad (11)$$

$$2H^+ + 2e^- \leftrightarrow H_2 \quad (12)$$

$$2H_2O + 2e^- \leftrightarrow H_2 + 2OH^- \quad (13)$$

The formation of $Fe_2(OH)_2CO_3$, as depicted in Eqs. (14-15), and its corresponding reaction mechanism illustrated in Fig. 14, was influenced by the concentrations of Fe^{2+}, OH^-, and HCO_3^-/CO_3^{2-} in the solution. The establishment of the protective $Fe_2(OH)_2CO_3$ layer was contingent upon specific concentration ratios; notably, a ratio of $[Fe^{2+}]/[OH^-]$ exceeding 1 and $[CO_3^{2-}]/[OH^-]$ surpassing 0.5 were pivotal for this process, as supported by previous research (Azoulay et al., 2012; Rémazeilles and Refait, 2009).

$$Fe^{2+} + OH^- \leftrightarrow Fe(OH)^+ \quad (14)$$

$$2Fe(OH)^+ + CO_3^{2-} \leftrightarrow Fe_2(OH)_2CO_3 \quad (15)$$

The absorption reactions involving amines, CO_2, and H_2O in this study can be described through two reactions: the formation of carbamate (Eq. (16)) and the subsequent hydrolysis of carbamate ions (Eq. (17)) (Buvik et al., 2021). These reactions created the corrosive conditions. The extent of corrosion was primarily determined by the concentration of HCO_3^-/CO_3^- ions in the solution. Fig. 15 shows the significant variation in the mole fraction of HCO_3^- ions in the 30 wt.% MEA and AMP-MEA blended solutions. In the MEA-CO_2 system, it is evident that the hydrolysis reaction of carbamate ions hardly occurred

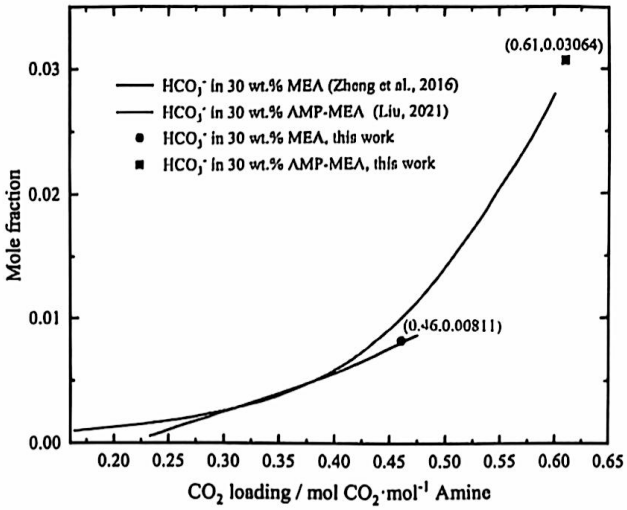

Fig. 15. Mole fraction of HCO_3^- in 30 wt.% MEA(Zheng et al., 2016a) and AMP-MEA blends (Liu, 2021) from reported work at 343 K, 1atm (curves) and data of this work (points).

unless the CO_2 loading was exceptionally high (Sánchez-Bautista et al., 2021). Conversely, the concentration of HCO_3^- ions in the AMP--MEA-CO_2 system exponentially increased with higher CO_2 loading. This disparity in HCO_3^- concentration between the two solvent systems accounted for the contrasting corrosion characteristics observed.

$$CO_2 + 2RR'NH \leftrightarrow RR'NCOO^- + RR'NH^+ \quad (16)$$

$$H_2O + RR'NCOO^- \leftrightarrow RR'NH + HCO_3^- \quad (17)$$

The EIS results revealed an increase in both solution resistance and charge transfer resistance to varying degrees following a 60-hour corrosion process of the carbon steel. Remarkably, in the solutions containing $NaVO_3$ and P-TEA, there was no discernible presence of a corrosion product layer on the surface of the carbon steel, underscoring their commendable corrosion resistance within the organic amine solution. Fig. 16 and Fig. 17 elucidate the corrosion inhibition mechanism of $NaVO_3$ and P-TEA, respectively. Intriguingly, the corrosion inhibition mechanism of $NaVO_3$ and P-TEA exhibited remarkable similarity. By virtue of electrostatic forces, $NaVO_3$ and P-TEA were drawn towards the metal surface, influencing the charged electrode region to effectively impede corrosion reactions (Bouyanzer et al., 2006). Both compounds outcompeted iron ions in the solution, forming complexes or chelates that adsorbed onto the carbon steel surface, thus preventing further corrosion reactions. Since corrosion initiated with the dissociation of CO_2 and its subsequent reaction with the amine solvent and metal surface, the formation of a stable film effectively hindered direct contact between corrosive ions in the solution, ultimately reducing the corrosion rate (LU et al., 2021; Srinivasan et al., 2013; Zhang et al., 2015; Zhao

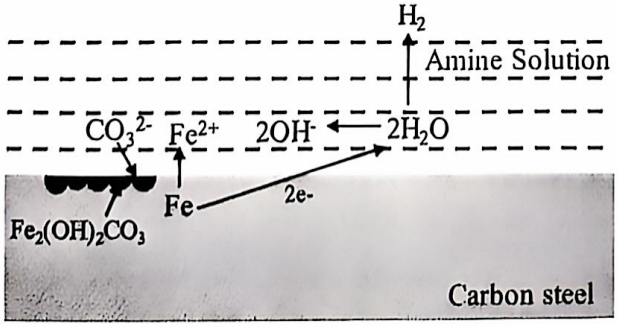

Fig. 14. Corrosion reaction mechanism diagram.

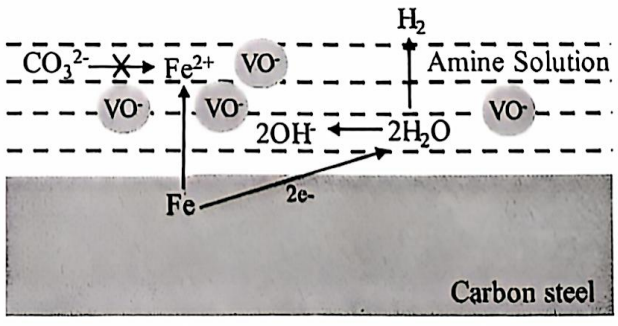

Fig. 16. Schematic diagram of $NaVO_3$ corrosion inhibition mechanism.

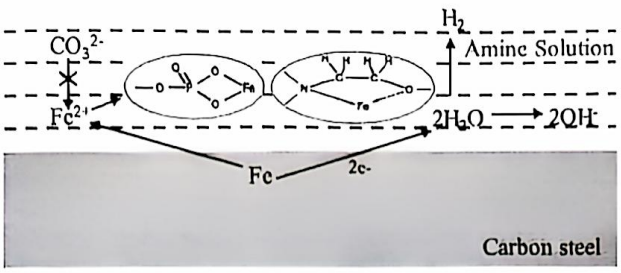

Fig. 17. Schematic diagram of P-TEA corrosion inhibition mechanism.

et al., 2023b).

As a prospect, atomic simulations are needed to give more insights into the inhibition mechanism of corrosion inhibitors on the metal surface at atomic and molecular scales since the information of metal-corrosion inhibitor interface interaction cannot be understood at the experimental level.

4. Conclusion

The corrosion behavior of A3 carbon steel in 30 wt.% MEA and AMP-MEA blended amine solutions, two typical CO_2 capture solvents for chemical absorption process, has been investigated. The inhibition effect of imidazoline, $NaVO_3$ and P-TEA in the two solvents were studied. According to the immersion corrosion experiment results, the corrosion rate of carbon steel stabilized after a sharp decrease in the first two weeks and the corrosion product coating on carbon steel was identified as $Fe_2(OH)_2CO_3$. AMP-MEA blends exhibited improved corrosion resistance, forming a denser $Fe_2(OH)_2CO_3$ protective layer on the surface of A3 carbon steel compared to the MEA solution at 100 °C. This was corroborated by the elevated bicarbonate concentration observed in the AMP-MEA solution. There was no notable discrepancy in the concentration of HSS anions and iron ions between the two solvent systems. The concentration hierarchy of HSS anions was sulfate > oxalate > glycolate > formate > acetate. Further comprehensive investigations are needed to delve into the corrosion behaviors of different blended amine solutions, particularly in relation to potential synergetic effects.

At a concentration level of 1000 ppm, $NaVO_3$ demonstrated the most effective corrosion inhibition, while imidazoline exhibited limited effectiveness. The order of corrosion inhibition effectiveness was $NaVO_3$ > *P*-TEA > imidazoline. This is attributed to that imidazoline's high susceptibility to hydrolysis in high-temperature alkaline solvent environment. Tafel curves for the three inhibitors displayed varying degrees of rightward shift, indicating an increase in corrosion potential. EIS results showed that the three inhibitors, to a certain extent, elevated the solution resistance and charge transfer resistance in the MEA system, achieving a corrosion inhibition effect. After 60-hour immersion corrosion, both solution and charge transfer resistances noticeably increased. The inhibition mechanisms of $NaVO_3$ and P-TEA were similar, involving competition with CO_3^{2-} ions and chelation with iron ions. It is worth noting that excessively high concentrations of corrosion inhibitors may lead to issues such as plugging and erosion. Therefore, further investigation is necessary to determine the optimal concentration for each corrosion inhibitor.

CRediT authorship contribution statement

Yuwei Wang: Writing – original draft, Software, Methodology, Investigation, Formal analysis, Conceptualization. **Mengxiang Fang:** Writing – review & editing, Supervision, Resources, Funding acquisition, Conceptualization. **Jun Gao:** Visualization, Validation, Investigation. **Chao Li:** Writing – review & editing, Resources, Funding acquisition. **Yan Huang:** Writing – review & editing, Methodology, Investigation. **Lin Yang:** Supervision, Data curation. **Shuifei Li:** Supervision, Resources, Funding acquisition, Conceptualization. **Ximing Hu:** Validation, Data curation. **Tao Wang:** Writing – review & editing, Investigation.

Declaration of competing interest

The authors declare that they have no known competing financial interests or personal relationships that could have appeared to influence the work reported in this paper.

Data availability

Data will be made available on request.

Acknowledgement

This work is supported by National Key R&D Program of China (2023YFE0199300), Pioneer R&D Program of Zhejiang Province-China (2022C03040) and the Fundamental Research Funds for the Central Universities (2022ZFJH004).

References

Kohl, A., Nielsen, R., 2007. Gas purification. Chem. Eng. 114 https://doi.org/10.1007/978-3-319-17668-0_42.

Ahn, S., Song, H.J., Park, J.W., Lee, J.H., Lee, I.Y., Jang, K.R., 2010. Characterization of metal corrosion by aqueous amino acid salts for the capture of CO2. Korean J. Chem. Eng. 27, 1576–1580. https://doi.org/10.1007/s11814-010-0246-z.

ASTM, 1999. Standard Guide for Conducting Corrosion Coupon Test in Field Applications 46.

Standard, A.S.T.M., 2011. G1-03: Standard practice For preparing, cleaning, and Evaluating Corrosion Test Specimens. ASTM Int.

Azoulay, I., Rémazeilles, C., Refait, P., 2012. Determination of standard Gibbs free energy of formation of chukanovite and Pourbaix diagrams of iron in carbonated media. Corros. Sci. 58, 229–236. https://doi.org/10.1016/j.corsci.2012.01.033.

Bouyanzer, A., Hammouti, B., Majidi, L., 2006. Pennyroyal oil from Mentha pulegium as corrosion inhibitor for steel in 1 M HCl. Mater. Lett. 60, 2840–2843. https://doi.org/10.1016/j.matlet.2006.01.103.

Buvik, V., Wanderley, R.R., Knuutila, H.K., 2021. Addition of potassium iodide reduces oxidative degradation of monoethanolamine (MEA). Chem. Eng. Sci. X 10, 100096. https://doi.org/10.1016/j.cesx.2021.100096.

Campbell, K.L.S., Zhao, Y., Hall, J.J., Williams, D.R., 2016. The effect of CO2-loaded amine solvents on the corrosion of a carbon steel stripper. Int. J. Greenh. Gas Control 47, 376–385. https://doi.org/10.1016/j.ijggc.2016.02.011.

Chen, Y.J., Jiang, L.H., Yan, X.C., Song, Z.J., Guo, M.Z., Zhao, S.J., Gong, W.S., 2020. Impact of phosphate corrosion inhibitors on chloride binding and release in cement pastes. Constr. Build. Mater. 236 https://doi.org/10.1016/j.conbuildmat.2019.117469.

Cousins, A., Ilyushechkin, A., Pearson, P., Cottrell, A., Huang, S., Feron, P.H.M., 2013. Corrosion coupon evaluation under pilot-scale CO2 capture conditions at an Australian coal-fi red power station. Greenh. Gases Sci. Technol. 3, 169–184. https://doi.org/10.1002/ghg.1341.

Emori, W., Jiang, S.L., Duan, D.L., Ekerenam, O.O., Zheng, Y.G., Okafor, P.C., Qiao, Y.X., 2017. Corrosion behavior of carbon steel in amine-based CO2 capture system: effect of sodium sulfite and sodium sulfite contaminants. Mater. Corros. 68, 674–682. https://doi.org/10.1002/maco.201609245.

Fytianos, G., Grimstvedt, A., Knuutila, H., Svendsen, H.F., 2014. Effect of MEA's degradation products on corrosion at CO2 capture plants. Energy Procedia 63, 1869–1875. https://doi.org/10.1016/j.egypro.2014.11.195.

Fytianos, G., Ucar, S., Grimstvedt, A., Hyldbakk, A., Svendsen, H.F., Knuutila, H.K., 2016. Corrosion and degradation in MEA based post-combustion CO2 capture. Int. J. Greenh. Gas Control 46, 48–56. https://doi.org/10.1016/j.ijggc.2015.12.028.

Gao, J., Wang, S., Sun, C., Zhao, B., Chen, C., 2012. Corrosion behavior of carbon steel at typical positions of an amine-based CO2 capture pilot plant. Ind. Eng. Chem. Res. 51, 6714–6721. https://doi.org/10.1021/ie203045v.

Gunasekaran, P., Veawab, A., Aroonwilas, A., 2013. Corrosivity of single and blended amines in CO2 capture process. Energy Procedia 37, 2094–2099. https://doi.org/10.1016/j.egypro.2013.06.088.

Hermas, A.E.A., Elnady, A.M., Ali, R.M., 2019. Corrosion inhibition of stainless steel in sulfuric acid solution containing sulfide ions. Anti-Corrosion Methods Mater 66, 360–368. https://doi.org/10.1108/ACMM-10-2018-2016.

Intergovernmental Panel on Climate Change, 2011. IPCC special report on carbon dioxide capture and storage. Environ. Sci. Technol. 45, 5710–5716.

Kittel, J., Gonzalez, S., 2014. Corrosion in CO2 post-combustion capture with alkanolamines – a review. Oil Gas Sci. Technol. 69, 915–929. https://doi.org/10.2516/ogst/2013161.

Kladkaew, N., Idem, R., Tontiwachwuthikul, P., Saiwan, C., 2009. Corrosion behavior of carbon steel in the monoethanolamine-H 2O-CO2-O2-SO2 system: products, reaction

pathways, and kinetics. Ind. Eng. Chem. Res. 48, 10169–10179. https://doi.org/10.1021/ie900746g.
Koo, T.H., Kim, J., 2020. Controls on the formation and stability of siderite (FeCo3) and chukanovite (Fe2(CO3)(OH)2) in reducing environment. Minerals 10. https://doi.org/10.3390/min10020156.
Lee, T.R., Wilkin, R.T., 2010. Iron hydroxy carbonate formation in zerovalent iron permeable reactive barriers: characterization and evaluation of phase stability. J. Contam. Hydrol. 116, 47–57. https://doi.org/10.1016/j.jconhyd.2010.05.009.
Liu, C.-T., Rochelle, G., 2022. Stainless and carbon steel corrosion in aqueous piperazine at absorber and water wash conditions. SSRN Electron. J. https://doi.org/10.2139/ssrn.4281844.
Liu, C.T., Fischer, K.B., Rochelle, G.T., 2019. Corrosion of carbon steel by aqueous piperazine protected by FeCO3. Int. J. Greenh. Gas Control 85, 23–29. https://doi.org/10.1016/j.ijggc.2019.03.027.
Liu, Z., 2021. Research On Mixed Absorbent and Optiminztion of CO2 Capture Process. Zhejiang University. https://doi.org/10.27461/d.cnki.gzjdx.2021.000057.
LU, Y., Shijun, L., Bowen, G., Liming, H., Ling, L., Fu, C., 2021. Corrosiveness analysis and corrosion inhibitor development of CO2 capture absorbent for flue gas. Nat. GAS Chem. Ind. 46, 102–105.
Al-Marri, M.J., A.B.C.N.T.S.R.I.C.S.P.T, 2017. Advancement and new perspectives of using formulated reactive amine blends for post-combustion carbon dioxide (CO2) capture technologies. Petroleum 3, 10–36. https://doi.org/10.1016/j.petlm.2016.11.002.
Ma, I.A.W., Ammar, S., Kumar, S.S.A., Ramesh, K., Ramesh, S., 2022. A concise review on corrosion inhibitors: types, mechanisms and electrochemical evaluation studies. J. Coatings Technol. Res. 19, 241–268. https://doi.org/10.1007/s11998-021-00547-0.
Nahali, H., Dhouibi, L., Idrissi, H., 2015. Effect of Na3PO4 addition in mortar on steel reinforcement corrosion behavior in 3% NaCl solution. Constr. Build. Mater. 78, 92–101. https://doi.org/10.1016/j.conbuildmat.2014.12.099.
Pandarinathan, V., Lepkova, K., van Bronswijk, W., 2014. Chukanovite (Fe2(OH)2CO3) identified as a corrosion product at sand-deposited carbon steel in CO2-saturated brine. Corros. Sci. 85, 26–32. https://doi.org/10.1016/j.corsci.2014.03.032.
Rémazeilles, C., Refait, P., 2009. Fe(II) hydroxycarbonate Fe2(OH)2CO3 (chukanovite) as iron corrosion product: synthesis and study by Fourier Transform Infrared Spectroscopy. Polyhedron 28, 749–756. https://doi.org/10.1016/j.poly.2008.12.034.
Romeo, L.M., Abanades, J.C., Escosa, J.M., Paño, J., Giménez, A., Sánchez-Biezma, A., Ballesteros, J.C., 2008. Oxyfuel carbonation/calcination cycle for low cost CO2 capture in existing power plants. Energy Convers. Manag. 49, 2809–2814. https://doi.org/10.1016/j.enconman.2008.03.022.
Rooney, P.C., Dupart, M.S., 2000. Corrosion in alkanolamine plants: causes and minimization. In: Proc. NACE - Int. Corros. Conf. Ser. 2000-March.
Sadeek, S.A., Williams, D.R., Sedransk Campbell, K.L., 2018. Using sodium thiosulphate for carbon steel corrosion protection against monoethanolamine and methyldiethanolamine. Int. J. Greenh. Gas Control 74, 206–218. https://doi.org/10.1016/j.ijggc.2018.05.005.
Saeed, L.M., Alaba, P., Mazari, S.A., Basirun, W.J., Lee, V.S., Sabzoi, N., 2018. Opportunities and challenges in the development of monoethanolamine and its blends for post-combustion CO2 capture. Int. J. Greenh. Gas Control 79, 212–233. https://doi.org/10.1016/j.ijggc.2018.11.002.
Saheb, M., Gallien, J.P., Descostes, M., Raimbault, L., Perez, A., Neff, D., Marsal, F., Pellegrini, D., Dillmann, P., 2014. Influence of an aerated/anoxic transient phase on the long-term corrosion of iron. Corros. Sci. 86, 71–80. https://doi.org/10.1016/j.corsci.2014.04.040.
Sánchez-Bautista, A., Palmero, E.M., Moya, A.J., Gómez-Díaz, D., La Rubia, M.D., 2021. Characterization of alkanolamine blends for carbon dioxide absorption. Corrosion and regeneration studies. Sustainability 13. https://doi.org/10.3390/su13074011.
Schlegel, M.L., Bataillon, C., Blanc, C., Prêt, D., Eddy, F., 2010. Anodic activation of iron corrosion in clay media under water-saturated conditions at 90 °C: characterization of the corrosion interface. Environ. Sci. Technol. 44, 1503–1508. https://doi.org/10.1021/es9021987.
Schweitzer, P.A., 2017. Atmospheric corrosion. Corros. Corros. Prot. Handbook, Second Ed, pp. 23–32. https://doi.org/10.1201/9781315140384.
Sedik, A., Athmani, S., Saoudi, A., Ferkous, H., Ribouh, N., Lerari, D., Bachari, K., Djellali, S., Berredjem, M., Solmaz, R., Alam, M., Jeon, B.H., Benguerba, Y., 2022. Experimental and theoretical insights into copper corrosion inhibition by protonated amino-acids. RSC Adv. 12, 23718–23735. https://doi.org/10.1039/d2ra03535a.
Shoukat, U., Knuutila, H.K., 2020. Effect of various parameters on the thermal stability and corrosion of CO2-loaded tertiary amine blends. Energies 13. https://doi.org/10.3390/en13102626.
Soosaiprakasam, I.R., Veawab, A., 2008. Corrosion and polarization behavior of carbon steel in MEA-based CO2 capture process. Int. J. Greenh. Gas Control 2, 553–562. https://doi.org/10.1016/j.ijggc.2008.02.009.
Srinivasan, S., Veawab, A., Aroonwilas, A., 2013. Low toxic corrosion inhibitors for amine-based CO2 capture process. Energy Procedia 37, 890–895. https://doi.org/10.1016/j.egypro.2013.05.182.
Stansbury, E.E., Buchanan, R.A., 2000. Fundamentals of electrochemical corrosion. Fundam. Electrochem. Corros. https://doi.org/10.31399/asm.tb.fec.9781627083027.
Tang, Y., Guo, X.P., Zhang, G.A., 2017. Corrosion behaviour of X65 carbon steel in supercritical-CO2 containing H2O and O2 in carbon capture and storage (CCS) technology. Corros. Sci. 118, 118–128. https://doi.org/10.1016/j.corsci.2017.01.028.
Tie, Z., Wei, Z., Zhao, J., 2017. Hydrolysis of an imidazoline corrosion inhibitor under different conditions. J. Beijing Univ. Chem. Technol. 44, 66–71. https://doi.org/10.13543/j.bhxbzr.2017.05.010.
Tsouris, C., Aaron, D., 2005. Separation of CO2 from flue gas: a review. Sep. Sci. Technol. 40, 321–348.
Veawab, A., Aroonwilas, A., 2002. Identification of oxidizing agents in aqueous amine-CO2 systems using a mechanistic corrosion model. Corros. Sci. 44, 967–987. https://doi.org/10.1016/S0010-938X(01)00125-1.
Veawab, A., Tontiwachwuthikul, P., Bhole, S.D., 1997. Studies of corrosion and corrosion control in a CO 2 −2-Amino-2-methyl-1-propanol (AMP) environment. Ind. Eng. Chem. Res. 36, 264–269. https://doi.org/10.1021/ie9504563.
Xiang, Y., Choi, Y.S., Yang, Y., Nešić, S., 2015. Corrosion of carbon steel in MDEA-based CO2 capture plants under regenerator conditions: effects of O2and heat-stable salts. Corrosion 71, 30–37. https://doi.org/10.5006/1354.
Xiang, Y., Yan, M., Choi, Y.S., Young, D., Nesic, S., 2014. Time-dependent electrochemical behavior of carbon steel in MEA-based CO2 capture process. Int. J. Greenh. Gas Control 30, 125–132. https://doi.org/10.1016/j.ijggc.2014.09.003.
Yadav, M., Kumar, S., Sharma, D., 2014. Studies on synthesized nontoxic corrosion inhibitors for N80 steel in hydrochloric acid. Anti-Corrosion Methods Mater 61, 129–138. https://doi.org/10.1108/ACMM-12-2012-1225.
Yan, Y., Wang, X., Zhang, Y., Wang, P., Cao, X., Zhang, J., 2013. Molecular dynamics simulation of corrosive species diffusion in imidazoline inhibitor films with different alkyl chain length. Corros. Sci. 73, 123–129. https://doi.org/10.1016/j.corsci.2013.03.031.
Yu, L.C.Y., Sadeek, S., Williams, D.R., Campbell, K.L.S., 2017. Investigating the corrosion due to high capacity and uptake promoter amine blends on carbon steel. Energy Procedia 114, 1998–2008. https://doi.org/10.1016/j.egypro.2017.03.1334.
Yu, L.C.Y., Sedransk Campbell, K.L., Williams, D.R., 2016. Using carbon steel in the stripper and reboiler for post-Combustion CO2 capture with aqueous amine blends. Int. J. Greenh. Gas Control 51, 380–393. https://doi.org/10.1016/j.ijggc.2016.04.031.
Zhang, H.H., Pang, X., Zhou, M., Liu, C., Wei, L., Gao, K., 2015. The behavior of pre-corrosion effect on the performance of imidazoline-based inhibitor in 3 wt.% NaCl solution saturated with CO 2. Appl. Surf. Sci. 356, 63–72. https://doi.org/10.1016/j.apsusc.2015.08.003.
Zhang, J., Liu, J., Yu, W., Yan, Y., You, L., Liu, L., 2010. Molecular modeling of the inhibition mechanism of 1-(2-aminoethyl)-2-alkyl-imidazoline. Corros. Sci. 52, 2059–2065. https://doi.org/10.1016/j.corsci.2010.02.018.
Zhao, B., Sun, Y., Yuan, Y., Gao, J., Wang, S., Zhuo, Y., Chen, C., 2011. Study on corrosion in CO2 chemical absorption process using amine solution. Energy Procedia 4, 93–100. https://doi.org/10.1016/j.egypro.2011.01.028.
Zhao, F., Cui, C., Dong, S., Xu, X., Liu, H., 2023a. An overview on the corrosion mechanisms and inhibition techniques for amine-based post-combustion carbon capture process. Sep. Purif. Technol. 304, 122091 https://doi.org/10.1016/j.seppur.2022.122091.
Zhao, F., Cui, C., Dong, S., Xu, X., Liu, H., 2023b. An overview on the corrosion mechanisms and inhibition techniques for amine-based post-combustion carbon capture process. Sep. Purif. Technol. 304, 122091 https://doi.org/10.1016/j.seppur.2022.122091.
Zheng, L., Landon, J., Zou, W., Liu, K., 2014. Corrosion benefits of piperazine as an alternative CO2 capture solvent. Ind. Eng. Chem. Res. 53, 11740–11746. https://doi.org/10.1021/IE501346Z.
Zheng, L., Matin, N.S., Landon, J., Thomas, G.A., Liu, K., 2016a. CO2 loading-dependent corrosion of carbon steel and formation of corrosion products in anoxic 30 wt.% monoethanolamine-based solutions. Corros. Sci. 102, 44–54. https://doi.org/10.1016/j.corsci.2015.09.015.
Zheng, L., Matin, N.S., Thompson, J., Landon, J., Holubowitch, N.E., Liu, K., 2016b. Understanding the corrosion of CO2-loaded 2-amino-2-methyl-1-propanol solutions assisted by thermodynamic modeling. Int. J. Greenh. Gas Control 54, 211–218. https://doi.org/10.1016/j.ijggc.2016.09.005.
Zhou, Y., Zuo, Y., Lin, B., 2017. The compounded inhibition of sodium molybdate and benzotriazole on pitting corrosion of Q235 steel in NaCl + NaHCO 3 solution. Mater. Chem. Phys. 192, 86–93. https://doi.org/10.1016/j.matchemphys.2017.01.083.
Zhou, Z., Guo, B., Lv, B., Guo, H., Jing, G., 2016. Performance and reaction kinetics of CO2 absorption into AMP solution with [Hmim][Gly] activator. Int. J. Greenh. Gas Control 44, 115–123. https://doi.org/10.1016/j.ijggc.2015.11.010.
Zhu, Y., Ping, Y., Liao, D., Wang, C., Luo, Y., 2002. Film formation mechanism of corrosion inhibitor imidazoline for carbon steel in high temperature alkaline solution. Materials Protection(Chinese) 35.